Chinese Physics Letters

LETTER

Electron–Phonon Coupling Drives the Gapless Charge Density Wave in Few-Layer 1T-VSe_2

Cite as: Yonglong Cheng *et al*. 2026 *Chin. Phys. Lett.* **43** 110802

DOI CSTR

Recommended Articles

Charge Density Wave Induced Second-Harmonic Generation in 1T-$TaSe_2$

Zhao-Zhe Chen, Chang-Hua Li, Hai-Xia Zhu, Yan-Peng Qi, and Si Xiao
Chin. Phys. Lett. **43**, 080404 (2026)

Photodoping-Modified Charge Density Wave Phase Transition in WS_2/1T-TaS_2 Heterostructure

Rui Wang, Jianwei Ding, Fei Sun, Jimin Zhao, and Xiaohui Qiu
Chin. Phys. Lett. **41**, (2024)

Revealing Light-Induced Charge Density Wave Melting and Carrier Redistribution in 1T-$TiSe_2$

Wanying Chen, Haoyuan Zhong, Changhua Bao, Fei Wang, Xuanxi Cai, Chenxia Yun, Hao Teng, Zhiyi Wei, and Shuyun Zhou
Chin. Phys. Lett. **42**, 017101 (2025)

Coexisting Commensurate Pair Density Waves in 6R-TaS_2

Hongqin Xiao, Yuxuan He, Ke Zhu, Yuhan Ye, Yumeng Li, Lijing Huang, Pucen Xiong, Haitao Yang, Geng Li, and Hong-Jun Gao
Chin. Phys. Lett. **43**, 060713 (2026)

Ultrafast Melting of Charge-Density-Wave Order and a Transient Metastable State in $4H_b$-TaS_2

Lingxiao Gu *et al*.
Chin. Phys. Lett. **43**, 090707 (2026)

Theory for Charge Density Wave and Orbital-Flux State in Antiferromagnetic Kagome Metal FeGe

Hai-Yang Ma, Jia-Xin Yin, M. Zahid Hasan, and Jianpeng Liu
Chin. Phys. Lett. **41**, (2024)

A series journal of Chinese Physical Society distributed by IOP Publishing

Chinese Physics Letters

Chin. Phys. Lett. **43** 110802 (2026)

LETTER

DOI: 10.1088/0256-307X/43/11/110802
CSTR: 32039.14.0256-307X.43.11.110802

Electron–Phonon Coupling Drives the Gapless Charge Density Wave in Few-Layer 1T-VSe_2

Yonglong Cheng(程咏龙), Yimanqi He(何逸蔓奇), and Xiangfan Xu(徐象繁)*

Center for Phononics and Thermal Energy Science, School of Physics Science and Engineering, Tongji University, Shanghai 200092, China

*Corresponding author. Email: xuxiangfan@tongji.edu.cn

The driving mechanism of the charge density wave (CDW) remains debated, particularly between Fermi surface nesting (FSN) and electron–phonon coupling (EPC) scenarios. Here, gate-tunable electrical and thermoelectric transport measurements were used to probe the CDW-related electronic structure in few-layer 1T-VSe_2. Thickness reduction strongly suppresses the long-range three-dimensional CDW order associated with the bulk transition near 110 K, allowing the high-temperature CDW-related anomaly near 170 K to be resolved in macroscopic transport. Through gate tuning, we find that this CDW-related state does not exhibit signatures of a well-defined Peierls-like gap but instead remains gapless within an intrinsic multiband electronic landscape. In particular, the Seebeck coefficient shows pronounced anomalies at both temperature scales (110 K and 170 K), yet no gap-induced thermoelectric anomaly or gate-dependent gap-opening behavior is observed. These results demonstrate the gapless nature of the CDW state, while the high-temperature 170 K anomaly directly fingerprints the localized precursor lattice softening, collectively providing strong transport evidence that supports EPC over conventional FSN as the dominant driving mechanism. Our work provides a new experimental perspective on the dimensionality-dependent CDW behavior in VSe_2 and establishes thermoelectric transport as a sensitive probe for distinguishing CDW formation mechanisms in low-dimensional materials.

The microscopic origin of charge-density-wave (CDW) order has long been a central issue in condensed matter physics [1–3]. In the conventional Peierls picture, CDW formation is driven by Fermi surface nesting (FSN), which enhances the electronic susceptibility at a characteristic wave vector and induces a coupled lattice distortion. However, increasing evidence indicates that CDW formation in many materials cannot be fully explained by a simple nesting scenario, and that lattice instability, electron correlations, and electron–phonon coupling (EPC) may play essential roles [4–9].

Transition-metal dichalcogenides (TMDs) provide an important platform for examining this issue, because their layered structures, tunable dimensionality, and strong coupling between electronic and lattice degrees of freedom give rise to rich CDW phenomena [10–17]. Among the 1T-structured TMDs, 1T-VSe_2 is a notable example. In particular, epitaxial monolayer 1T-VSe_2 has been reported to host multiple CDW phases, highlighting the rich dimensionality-dependent CDW physics in this material [13]. Bulk 1T-VSe_2 exhibits a CDW transition near $T_{CDW} \approx 110$ K, while the corresponding transport anomaly is unusually weak and the system remains metallic across the transition [18,19]. The microscopic origin of this reconstruction remains under debate. Early angle-resolved photoemission spectroscopy (ARPES) measurements reported a partial gap of about 20–30 meV near the M point and interpreted it in terms of a nesting-related instability [20]. This scenario was further supported by soft-X-ray ARPES measurements, which proposed a three-dimensional FSN mechanism [21]. In contrast, theoretical and structural studies have pointed to important roles of lattice effects, structural instability, and EPC in CDW formation [22–24]. More recent studies further suggest that the CDW state of 1T-VSe_2 involves a multiband electronic structure that is not easily reconciled with a simple Peierls picture [25].

In this work, we investigate the electronic structure and driving mechanism of the CDW state in few-layer 1T-VSe_2 in the two-dimensional limit by combining gate-tunable transport and thermoelectric measurements. A 5.6-nm-thick device shows metallic transport with a resistance anomaly near 170 K, suggesting the presence of a high-temperature CDW precursor phase. Gate-dependent resistance exhibits a nonmonotonic double-peak feature, indicating intrinsic multiband behavior near the Fermi level. The Seebeck coefficient evolves continuously with gate voltage and temperature, without the gap-opening signature expected for an FSN-driven Peierls transition. Thermoelectric measurements further resolve anomalies near 170 K and 110 K, associated with the CDW precursor phase and residual three-dimensional CDW correlations, respectively. These results suggest that CDW-related states in few-layer 1T-VSe_2 are gapless and are more likely governed by strong EPC than conventional FSN.

To investigate the transport properties of the CDW state in few-layer VSe_2, we initially prepared high-quality thin-layer nanosheets on a SiO_2/Si substrate via the mechanical exfoliation method. Subsequently, we fabricated micro-nano devices for precise measurement using electron beam lithography (EBL) technology, as depicted in Fig. 1(a). The thermoelectric measurement process is shown in Fig. 1(b). The two thermometers were placed near opposite sides of the VSe_2 channel to determine the local temperature gradient. Before measurements, the resistivity of each thermometer was calibrated as a function of temperature. A heating current was applied to the microheater to generate an in-plane temperature difference across the VSe_2 channel. The local temperatures T_{hot} and T_{cold} were extracted from the calibrated thermometer resistivity, and the temperature difference was obtained as $\Delta T = T_{hot} - T_{cold}$. The thermovoltage ΔV_S was measured between the voltage probes under open-circuit conditions, and the Seebeck coefficient was calculated using $S = -\Delta V_S / \Delta T$. Gate-dependent Seebeck measurements were performed by sweeping V_{BG} at fixed temperatures, while temperature-dependent measurements were conducted across the transition regime.

Figure 1(c) shows the Raman spectra of the mechanically exfoliated 1T-VSe_2 flake before and after laser-induced oxidation. The pristine sample exhibits a dominant Raman peak near 210 cm^{-1}, consistent with the characteristic Raman response of multilayer 1T-VSe_2 reported previously [26]. The absence of additional oxidation-related peaks in the pristine spectrum indicates that the mechanically exfoliated flake maintains good structural quality. After increasing the laser power, new Raman features emerge, especially around 250–260 cm^{-1},

Received 21 July 2026; accepted 10 October 2026; published 5 November 2026

© 2026 Chinese Physical Society and IOP Publishing Ltd. All rights, including for text and data mining, AI training, and similar technologies, are reserved.

Check for updates

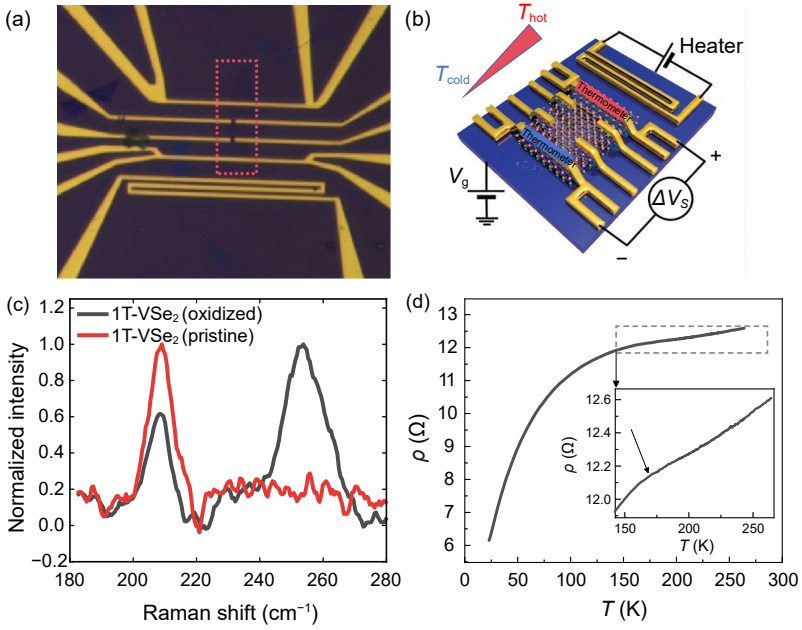

Fig. 1. (a) Optical image of the mechanically exfoliated device after electron-beam lithography (EBL) fabrication. The red dashed line outlines the mechanically exfoliated sample. (b) Schematic illustration of the thermoelectric measurement configuration. (c) Raman spectra of the mechanically exfoliated sample before and after laser-induced oxidation using increased laser power. (d) Temperature-dependent electrical resistivity ρ measured from 20 K to 270 K, showing typical metallic behavior. The inset shows a magnified view of the dashed-box region. A subtle kink appears near $T_{CDW} \approx 170$ K.

which can be attributed to oxidation-induced vibrational modes. The appearance of this oxidation peak is only observed in the 1T structure of VSe_2, and the characteristic peak of the 2H structure remains unchanged regardless of the degree of oxidation [26]. These results confirm that the exfoliated sample indeed possesses the 1T structure and maintains good quality after mechanical exfoliation.

Figure 1(d) presents the temperature dependence of the resistivity (ρ) of the device within the range from 20 K to 270 K. Throughout the entire testing temperature range, the system demonstrates typical metallic conduction behavior ($d\rho/dT > 0$). In our 5.6 nm (approximately 9 layers) VSe_2 sample, a weak yet distinct change in the resistivity slope (kink) emerges at $T \approx 170$ K [Fig. 1(d), inset]. This disappearance of the bulk 110 K transition and the emergence of a higher-temperature correlation closely resemble the behaviors reported in monolayer and monolayer-limit VSe_2. For instance, Feng *et al*. observed an enhanced long-range 2D CDW order at 140 ± 5 K using ARPES and LEED [27], while Duvjir *et al*. reported that localized CDW-induced energy gaps and real-space modulations in STM/STS can persist up to approximately 350 K [28]. This wide temperature range (140–350 K) in the single-layer limit highlights that the reduced dimensionality can favor CDW-related correlations that survive at much higher temperatures than the bulk phase. The trend that the CDW strengthens as the number of layers decreases differs from the monotonic decrease of the CDW transition temperature with the decreasing thickness of few-layer samples reported by Yang *et al*. [29] and Liu *et al*. [30]. On one hand, this difference may be due to the influence of surface disorder in the early samples. On the other hand, it may suggest that as the dimensionality decreases, the interlayer coupling gradually weakens, and the coherence that originally supported the $4a \times 4a \times 3c$ three-dimensional long-range CDW order in the bulk phase also gradually vanishes. Consequently, the three-dimensional CDW transport anomaly at approximately 110 K is significantly weakened or even completely disappears. Meanwhile, the local CDW precursor features hidden in the high-temperature region of the bulk phase also start to emerge in the transport measurements. The 170 K kink observed in our measurement can be naturally understood in light of recent structural diffraction studies. Temperature-dependent X-ray total scattering experiments by Petkov *et al*. indicate that the CDW formation in bulk 1T-VSe_2 is actually a two-step process: before the establishment of the 3D long-range $4a \times 4a \times 3c$ superstructure at $T_{CDW} \approx 110$ K, the system preemptively enters a CDW precursor phase (PF) at $T_{cdw}^{PF} \approx 200$ K [22]. In this precursor phase, the lattice softens, accompanied by local in-plane and out-of-plane static displacements of V and Se atoms. Therefore, the resistivity kink at ~170 K is precisely the intrinsic transport signature of this high-temperature precursor phase. The slight temperature difference between the ~200 K structural precursor in bulk 1T-VSe_2 [22] and the ~170 K transport anomaly in our few-layer device may stems from two factors. First, local structural probes capture short-range, sub-nanometer atomic displacements, whereas macroscopic transport anomalies require these distortions to develop spatial coherence to effectively scatter itinerant carriers. Second, thinning to the few-layer regime enhances low-dimensional fluctuations and weakens interlayer coupling, which typically suppresses the characteristic transition temperature compared to the 3D bulk [31].

Based on these findings, we can reconcile the intricate thickness dependence in VSe_2. As the thickness approaches the 2D limit, the interlayer coupling is suppressed, which effectively quenches the 3D CDW long-range order at approximately 110 K. In contrast, the precursor phase (at approximately 170 K in our sample), which is primarily driven by strong intralayer local electron–lattice coupling (e.g., local V-atom clustering) [22], shows remarkable robustness against dimensional reduction. This may imply that enhancement of T_{CDW} reported in monolayer VSe_2 (ranging from 140 K to 350 K) may essentially be the further stabilization of this high-temperature precursor phase in the ultimate 2D limit. Because this precursor phase does not open a macroscopic Peierls energy gap through FSN, but instead manifests as localized lattice distortions governed by strong EPC, its resistive signature is inherently subtle. This highlights the importance of combining gate-voltage-dependent transport with Seebeck coefficient measurements, the latter being highly sensitive to the energy derivative of the density of states, to clarify the electronic nature of the CDW state and its evolution across the transition.

To further explore the influence of the CDW precursor phase on the electronic structure, we firstly systematically measured the gate-voltage-tuned transport characteristics of the device at various temperatures. As depicted in Fig. 2(a), within the temperature range of 20 K to 150 K, we documented the evolution curves of the longitudinal resistivity ρ with respect to the back-gate voltage (V_{BG}, scanning range from −35 V to +35 V).

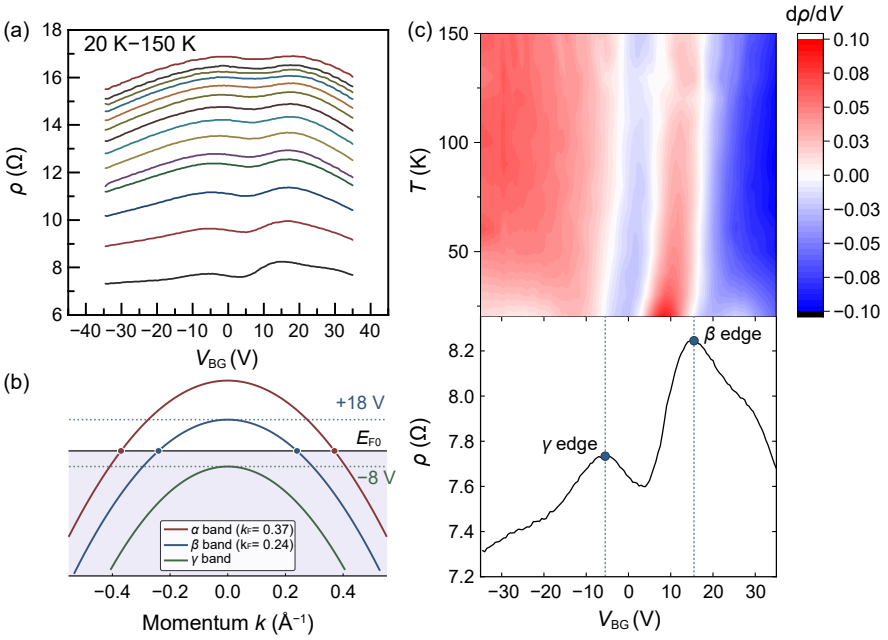

Fig. 2. Gate-tunable electrical transport measurements. (a) The longitudinal resistivity ρ as a function of the back-gate voltage V_{BG} within the temperature range from 20 K to 150 K. (b) Schematic low-energy bands of 1T-VSe_2 based on ARPES [25]. α and β subbands cross the Fermi level (E_{F0}), while γ band sits just below it. (c) A two-dimensional intensity map of the corresponding differential ($d\rho/dV_{BG}$) as a function of gate voltage and temperature. The following figure presents a schematic diagram depicting the β and γ band edge at 20 K.

Remarkably, the low-temperature ρ–V_{BG} curves display a highly anomalous, non-monotonic structure. The resistivity shows distinct double-hump profiles with local maxima at approximately $V_{BG} \approx -8$ V and +18 V, which directly demonstrates the macroscopic transport characteristics of a complex, multiband electronic structure near the Fermi level (E_F). The CDW generated via the FSN creates an energy gap in the vicinity of the Fermi surface, leading to a significant rise in resistivity near the charge neutral point. Nevertheless, the double-hump persists beyond 110 K, which further demonstrates that this CDW is not driven by FSN. This transport picture is perfectly corroborated by the recent high-resolution ARPES study by Yilmaz *et al.* [25], who unambiguously resolved a surprisingly rich multiband Fermi surface near the Γ point, identifying three closely lying subbands denoted as α, β, and γ. Importantly, Yilmaz *et al.* established that these subbands are intrinsic to the material and exist independently of the structural distortion. In our experiment, the field-effect gating acts as a dynamic electrostatic probe. As V_{BG} shifts E_F across the precise band edges of these localized subbands (for instance, tuning E_F into the γ band), the system experiences abrupt variations in the available density of states, directly translating into the resistivity hump we observe.

To more intuitively unveil the physical origin of the aforementioned non-monotonic gate voltage response, we further plotted a two-dimensional intensity map of the first-order derivative of resistivity with respect to the back-gate voltage, $d\rho/dV_{BG}$, as a function of temperature and gate voltage, as depicted in Fig. 2(c). In comparison with the original ρ–V_{BG} curve, the differential map can more distinctly highlight the positions where the resistivity varies most rapidly with the gate voltage. Thus, it can act as an effective approach for identifying the transport anomalies when the Fermi level traverses the band edge. Evidently, there are two prominent differential anomalies in the low-temperature region, situated near $V_{BG} \approx -8$ V and $V_{BG} \approx +18$ V, respectively. The ρ–V_{BG} curve at 20 K presented at the bottom of Fig. 2(c) further demonstrates that these two characteristic positions correspond to the two local maxima in the double-hump structure of the resistivity.

Combined with the energy band schematic diagram presented in Fig. 2(b), these two characteristic gate voltages can be respectively ascribed to the process where the Fermi level crosses the edges of the γ and β subbands. According to the existing ARPES research, there exist multiple subbands in the vicinity of the Fermi level around the Γ point in VSe_2, namely the α, β, and γ bands. When the carrier concentration is regulated by the back gate voltage, the Fermi level shifts relative to these subbands and successively sweeps across the edges of the γ and β subbands. Given that the density of states, scattering phase space, and multiband transport channels near the band edges undergo significant changes, the resistivity of the system rises near the corresponding gate voltages.

Therefore, figures 2(b) and 2(c) present a clearer multiband transport image of the double-hump structure in the low-temperature ρ–V_{BG} curve. Specifically, the double peaks in resistivity do not merely correspond to the single energy gap generated by the traditional FSN-driven CDW. Instead, they are more likely to reflect the reconstruction of low-energy electronic states resulting from the adjustment of the Fermi level among multiple neighboring subbands. Notably, these features can still be observed within a relatively wide temperature range, indicating that they are closely associated with the intrinsic multiband electronic structure of VSe_2 and may be further modulated by the local EPC in the CDW precursor phase.

The gate-voltage-dependent transport results in Fig. 2 suggest that the low-temperature double-hump structure originates from the intrinsic multiband electronic structure rather than from a conventional FSN-induced Peierls gap. However, resistivity is affected by both the density of states and scattering processes, making it difficult to fully resolve subtle electronic-structure changes near the Fermi level. To further distinguish between an FSN-driven gap-opening scenario and an EPC-driven gapless reconstruction, we turn to thermoelectric transport.

Figure 3(a) depicts the variation of the Seebeck coefficient (S) with back-gate voltage (V_{BG}, from −40 V to +40 V) at temperatures between 20 K and 260 K. The nature of the CDW in 1T-VSe_2 has been a subject of debate: early ARPES work by Terashima *et al.* [20] attributed the transition to conventional FSN and suggested a CDW gap of approximately 20 meV. In contrast, recent high-resolution ARPES investigations by Yilmaz *et al.* [25] demonstrated that the Fermi surface remains essentially gapless across the CDW transition, challenging the conventional Peierls scenario.

Based on the Mott relation $S \propto -\frac{d\ln[D(E)\cdot v^2(E)\tau(E)]}{dE}|_{E_F}$, where $D(E)$, $v(E)$, and $\tau(E)$ are the density of states, carrier velocity, and relaxation time, respectively [32,33], if a CDW gap on the order of 20–30 meV

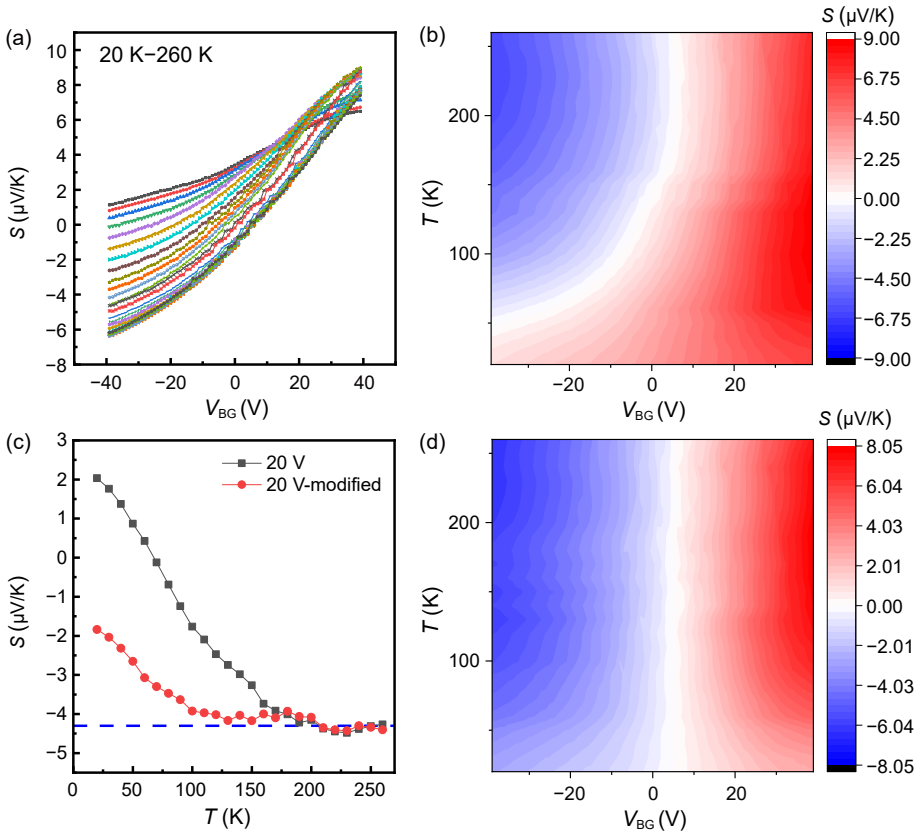

Fig. 3. Decoupling the thermoelectric signal and the determination of the EPC mechanism. (a) Variation of the thermoelectric coefficient (S) with gate voltage in the temperature range from 20 K to 260 K. (b) Raw 2D contour map of the Seebeck coefficient (S) as a function of V_{BG} and temperature. (c) Modified S vs. T at fixed hole-doping ($V_{BG} = -20$ V) (The data at different gate voltages are provided in the SM). (d) The modified phase diagram after subtracting the phenomenological subbands baseline.

[20] were to open, sweeping the chemical potential through this gap should induce a pronounced thermoelectric anomaly, such as a sharp peak, dip, or abrupt slope change. With our estimated gate-to-energy conversion rate ($\Delta\mu/\Delta V_{BG} \approx 1.5$ meV/V near the charge neutrality point), sweeping across a 20 meV energy window corresponds to a gate span of approximately 13 V, well within our ±40 V measurement window. Furthermore, at our base temperature of 20 K (deep in the CDW phase), the thermal broadening kernel exhibits a full width at half maximum of $3.53k_BT \approx 6$ meV. Because this thermal window is substantially narrower than the proposed 20 meV scale, a gap of that magnitude should not be fully obscured by thermal smearing.

Nevertheless, our measured $S(V_{BG})$ exhibits a completely smooth and monotonic evolution at 20 K without any gap-induced anomalies. This macroscopic transport result strongly supports the recent ARPES findings of Yilmaz *et al.* [25] and indicates the absence of a sizeable, transport-dominant global CDW gap in 1T-VSe_2. We note, however, that because thermoelectric transport measures a conductivity-weighted sum over all bands, an ultra-small gap (≤5 meV) below the thermal and disorder broadening threshold, or a partial gap strictly confined to an insensitive, low-mobility subband, cannot be entirely excluded by transport alone.

To further ascertain the origin of the CDW-related anomalies, we conducted a phenomenological analysis on the Seebeck data. As shown in Figs. 3(a) and 3(b), above 170 K, the position of the electrical neutral point of the Seebeck coefficient remains relatively stable around $V_{BG} \approx 6$ V, which suggests that the main energy band governing the transport does not exhibit an obvious shift with temperature. Therefore, we chose the Seebeck coefficient at $V_{BG} = 6$ V for each temperature as the background reference and corrected the original data as follows:

$$S_{\mathrm{mod}}(V_{BG}, T) = S(V_{BG}, T) - S(6\ \mathrm{V}, T). \quad (1)$$

Through this treatment, the additional thermoelectric response related to the multiband electronic structure can be separated to a certain extent.

Figure 3(c) presents a comparison between the original Seebeck data and the modified data at $V_{BG} = -20$ V. It is evident that the original data remains essentially flat above 170 K. However, below 170 K, it starts to deviate notably from the high-temperature plateau, and this deviation gradually intensifies as the temperature decreases. This characteristic temperature is in line with the temperature at which the resistivity curve exhibits a kink in Fig. 1(d), and therefore can be ascribed to the formation of the high-temperature CDW precursor phase. In other words, near 170 K, although the system has not yet established a traditional three-dimensional long-range CDW order, the local lattice distortion and EPC have begun to significantly modulate the electronic structure near the Fermi level, leading to a discernible anomaly in the Seebeck coefficient.

More intriguingly, the $S_{\mathrm{mod}}(T)$ curve after background subtraction also exhibits additional changes in the vicinity of 110 K. This temperature is close to the characteristic temperature associated with the three-dimensional CDW transition in bulk VSe_2. Hence, this low-temperature anomaly may reflect residual bulk-like CDW correlations or short-range CDW coherence in the 5.6-nm VSe_2 device. We emphasize that this feature is identified phenomenologically and should not be regarded as evidence for the recovery of a well-defined three-dimensional long-range CDW transition. In other words, even though the interlayer coupling is substantially weakened after thinning, which causes the traditional 110 K three-dimensional CDW to no longer display a strong phase-transition anomaly in the resistivity, residual three-dimensional CDW correlations or short-range CDW coherence may still contribute to the thermoelectric response.

Therefore, figure 3(c) actually reveals two different energy/temperature scales: the anomaly at the relatively high temperature of ~170 K corresponds to the CDW precursor phase dominated by EPC; while the feature at the lower temperature of ~110 K may be related to

the remaining three-dimensional CDW correlations. The temperature-dependent behavior at different gate voltages is presented in the Supplementary Materials (SM). This result supports the picture we proposed: in the thin-layer VSe_2, the long-range order of the traditional bulk-like three-dimensional CDW is significantly weakened, but the high-temperature precursor phase remains stable and significantly affects the thermoelectric transport by modulating the multiband electronic structure and scattering processes.

The above analysis of the cross-section at $V_{BG} = -20$ V can be further corroborated by the two-dimensional Seebeck distributions presented in Figs. 3(b) and 3(d). Figure 3(b) depicts a two-dimensional plot of the original S (V_{BG}, T). Above 170 K, the sign-reversal boundary remains essentially stable at around $V_{BG} \approx 6$ V. This stable boundary implies that the mainband background in the high-temperature region exhibits low sensitivity to temperature. Consequently, it is justifiable to adopt S(6 V, T) as the reference background. More crucially, the low-temperature enhancement observed at −20 V in Fig. 3(c) is not an incidental phenomenon at a single gate-voltage point. The most prominent characteristic in Fig. 3(d) is that the shape of the contour lines undergoes a significant alteration at approximately 110 K. Above 110 K, the overall shape of the S_{mod} contour lines remains largely similar, indicating that the gate-voltage dependence after background subtraction varies minimally with temperature. Conversely, below 110 K, the contour lines are no longer approximately vertical but display distinct bending or tilting, suggesting that the gate-voltage dependence of S_{mod} changes significantly in the low-temperature region. In other words, below 110 K, the thermoelectric response is no longer merely a translation along the temperature direction or an overall enhancement; instead, an electronic state reconstruction with gate-voltage selectivity takes place. Given that this temperature scale is close to the three-dimensional CDW transition temperature of bulk VSe_2, the evolution of non-vertical contour lines below 110 K in Fig. 3(d) may reflect the residual three-dimensional CDW correlations in the thin-layer sample.

It is important to emphasize that for the two distinct characteristic temperature scales in thermoelectric transport, neither the anomaly around 170 K nor the residual three-dimensional charge-density wave (CDW) near 110 K results in a sharp anomaly similar to the opening of an energy gap in the gate-voltage-dependent Seebeck curve. This finding is consistent with the absence of an FSN-type energy gap feature in the resistivity signal shown in Fig. 2. Therefore, the thermoelectric anomalies provide evidence for the existence of a gapless CDW state in few-layer 1T-VSe_2, which is consistent with the EPC driven mechanism and different from the traditional FSN picture.

In summary, we conducted a systematic investigation into the electrical and thermoelectric transport properties of few-layer 1T-VSe_2 to elucidate the nature of the CDW transition under two-dimensional conditions. As the layer thickness reduces, the three-dimensional long-range CDW order associated with the 110 K transition in the bulk phase is notably suppressed. This enables the high-temperature CDW-related electronic state reconstruction around 170 K to be more clearly revealed in macroscopic transport. Through gate-voltage tuning, we further verified that this reconstructed state evolves continuously within the material's intrinsic multiband electronic structure, without the formation of a well-defined Peierls-type energy gap. Importantly, as a probe that is highly sensitive to the electronic structure near the Fermi level, the Seebeck coefficient displays distinct thermoelectric anomalies at two characteristic temperature scales. However, there is no abrupt increase in the thermoelectric value due to the opening of an energy gap, nor does it exhibit the characteristics of gate-voltage-dependent energy-gap opening. Therefore, these results suggest that the CDW state in few-layer 1T-VSe_2 is gapless. The absence of a Peierls gap disfavors a conventional FSN mechanism, while the emergence of the 170 K anomaly correlates with the high-temperature precursor lattice softening. Together, these macroscopic transport findings provide compelling evidence supporting an EPC-dominated driving mechanism. Our work thus designates few-layer 1T-VSe_2 as a typical system for studying EPC-driven gapless CDW and demonstrates that gate-voltag-tunable thermoelectric transport is a powerful method for distinguishing different CDW formation mechanisms in low-dimensional quantum materials.

Acknowledgments

This work was supported by the National Key R&D Project from Ministry of Science and Technology of China (Grant No. 2024YFA1207900), the National Natural Science Foundation of China (Grant Nos. 12574039 and 12174286), and the Science and Technology Commission of Shanghai Municipality (Grant No. 26500713000).

References

[1] Zhu X, Cao Y, Zhang J, Plummer E W, and Guo J 2015 *Proc. Natl. Acad. Sci. U. S. A.* **112** 2367
[2] Boubeche M, Yu J, Chushan L, Huichao W, Zeng L, He Y, Wang X, Su W, Wang M, Yao D X, Wang Z, and Luo H 2021 *Chin. Phys. Lett.* **38** 037401
[3] Cao Z Y, Chen H, Qian G J, Shi Y H, Qi Q, Han X H, Yang H T, and Gao H J 2025 *Chin. Phys. Lett.* **42** 100702
[4] Wu L, Hu Y, Fan D, Wang D, and Wan X 2023 *Chin. Phys. Lett.* **40** 117103
[5] Xie X, Lin D, Zhu L, Li Q, Zong J, Chen W, Meng Q, Tian Q, Li S C, Xi X, Wang C, and Zhang Y 2021 *Chin. Phys. Lett.* **38** 107101
[6] Brouet V, Yang W L, Zhou X J, Hussain Z, Moore R G, He R, Lu D H, Shen Z X, Laverock J, Dugdale S B, Ru N, and Fisher I R 2008 *Phys. Rev. B* **77** 235104
[7] Yao C, Wen L, Zhao Y, Zhu Y, Wang Y, Tang G, Yan X, Zhang J, Huang Y, Sun H, Mao Z, Qi Y, Zheng Y, and Xing H 2024 *Phys. Rev. B* **110** 165136
[8] Chang J, Blackburn E, Holmes A T, Christensen N B, Larsen J, Mesot J, Liang R, Bonn D A, Hardy W N, Watenphul A, Zimmermann M V, Forgan E M, and Hayden S M 2012 *Nat. Phys.* **8** 871
[9] Ghiringhelli G, Le Tacon M, Minola M *et al*. 2012 *Science* **337** 821
[10] Rossnagel K 2011 *J. Phys. : Condens. Matter* **23** 213001
[11] Tu W, Lv R, Shao D, Sun Y, and Lu W 2025 *Chin. Phys. B* **34** 097103
[12] Zhu L, Zhao W M, Jia Z Y, Li H, Xie X, Li Q Y, Wang Q W, Dou L G, Hu J G, Zhang Y, Zhu W, Yu S L, Li J X, and Li S C 2023 *Chin. Phys. Lett.* **40** 057101
[13] Zong J, Xie Y, Meng Q, Tian Q, Chen W, Xie X, Jin S, Zhang Y, Wang L, Ren W, Shen J, Chen A, Wang P, Li F S, Dong Z, Wang C, Li J X, and Zhang Y 2022 *Chin. Phys. B* **31** 107301
[14] Wilson J A, Di Salvo F J, and Mahajan S 1974 *Phys. Rev. Lett.* **32** 882
[15] Mihailovic D, Dvorsek D, Kabanov V V, Demsar J, Forró L, and Berger H 2002 *Appl. Phys. Lett.* **80** 871
[16] Goli P, Khan J, Wickramaratne D, Lake R K, and Balandin A A 2012 *Nano Lett.* **12** 5941
[17] Adelman T L, Zaitsev-Zotov S V, and Thorne R E 1995 *Phys. Rev. Lett.* **74** 5264
[18] Whangbo M H and Canadell E 1992 *J. Am. Chem. Soc.* **114** 9587
[19] Bayard M and Sienko M J 1976 *J. Solid State Chem.* **19** 325
[20] Terashima K, Sato T, Komatsu H, Takahashi T, Maeda N, and Hayashi K 2003 *Phys. Rev. B* **68** 155108
[21] Strocov V N, Shi M, Kobayashi M, Monney C, Wang X, Krempasky J, Schmitt T, Patthey L, Berger H, and Blaha P 2012 *Phys. Rev. Lett.* **109** 086401
[22] Petkov V, Zafar A, Jakhar M, and Abeykoon A M 2025 *Phys. Rev. B* **111** 014105
[23] Diego J, Subires D, Said A H *et al*. 2024 *Phys. Rev. B* **109** 035133
[24] Johannes M D and Mazin I I 2008 *Phys. Rev. B* **77** 165135
[25] Yilmaz T, Vescovo E, and Sinkovic B 2023 *Phys. Rev. B* **107** 165109
[26] Li D, Wang X, Kan C, He D, Li Z, Hao Q, Zhao H, Wu C, Jin C, and Cui X 2020 *ACS Appl. Mater. Interfaces* **12** 25143
[27] Feng J, Biswas D, Rajan A *et al*. 2018 *Nano Lett.* **18** 4493
[28] Duvjir G, Choi B K, Jang I, Ulstrup S, Kang S, Thi Ly T, Kim S, Choi Y H, Jozwiak C, Bostwick A, Rotenberg E, Park J G, Sankar R, Kim K S, Kim J, and Chang Y J 2018 *Nano Lett.* **18** 5432
[29] Yang J, Wang W, Liu Y, Du H, Ning W, Zheng G, Jin C, Han Y, Wang N, Yang Z, Tian M, and Zhang Y 2014 *Appl. Phys. Lett.* **105** 063109
[30] Liu H, Bao L, Zhou Z, Che B, Zhang R, Bian C, Ma R, Wu L, Yang H, Li J, Gu C, Shen C M, Du S, and Gao H J 2019 *Nano Lett.* **19** 4551
[31] Tsen A W, Hovden R, Wang D, Kim Y D, Okamoto J, Spoth K A, Liu Y, Lu W, Sun Y, Hone J C, Kourkoutis L F, Kim P, and Pasupathy A N 2015 *Proc. Natl. Acad. Sci. U.S.A.* **112** 15054
[32] Jonson M and Mahan G D 1980 *Phys. Rev. B* **21** 4223
[33] Wu J, Chen Y, Wu J and Hippalgaonkar K 2018 *Adv. Electron. Mater.* **4** 1800248